Research Square

Preprints are preliminary reports that have not undergone peer review.
They should not be considered conclusive, used to inform clinical practice,
or referenced by the media as validated information.

Dynamic Stabilization of Biped Robots on Compound Terrains via Upper- Body Compensated Hybrid Switching ZMP Control

Arash Rahmani
Urmia University of Technology
Soheil Sheikh Ahmadi
soheil.sheikhahmadi@tabrizu.ac.ir
University of Tabriz
Mohammad Hatamnezhad
Urmia University of Technology

Research Article

Keywords: Biped robot, Zero Moment Point (ZMP), Dynamic stability regulation, Cubic spline modeling, Compound path locomotion, Upper-body compensation

Posted Date: November 13th, 2026

DOI: https://doi.org/10.21203/rs.3.rs-11383505/v1

License: This work is licensed under a Creative Commons Attribution 4.0 International License.
Read Full License

Additional Declarations: No competing interests reported.

Dynamic Stabilization of Biped Robots on Compound Terrains via Upper-Body Compensated Hybrid Switching ZMP Control

Arash Rahmani[1], Soheil Sheikh Ahmadi[2, *], Mohammad Hatamnezhad[1]

[1,]Department of Mechanical Engineering, Faculty of Mechanical Engineering, Urmia University of Technology, Urmia, Iran.

[2,] Control Engineering Department, Faculty of Electrical and Computer Engineering, University of Tabriz, Tabriz, Iran. soheil.sheikhahmadi@tabrizu.ac.ir

*Corresponding Author: Soheil Sheikh Ahmadi

Abstract: This paper presents a simulation-based study on dynamic stability control of a planar biped robot walking over compound terrains consisting of flat surfaces, inclined planes, and stair steps. The locomotion problem is modeled as a hybrid switching system, in which discrete transitions between single-support and double-support phases are coordinated through a phase-dependent switching control strategy. For each phase, smooth and continuous joint trajectories are generated using cubic spline interpolation. Dynamic balance is assessed and regulated through a Switching Zero- Moment Point (ZMP)-based criterion, where the admissible stability region is updated according to the active support phase and its corresponding support polygon. A key contribution of this work is the integration of upper-body mass compensation into the switching ZMP framework. By explicitly incorporating the torso contribution into the dynamic model and adjusting upper-body motion across gait transitions, corrective moments are generated to keep the ZMP within the admissible region under varying terrain conditions. Simulation results show that the proposed hybrid switching controller improves trajectory tracking, enhances ZMP regulation, and preserves stable locomotion across compound and uneven walking surfaces.

.

Keywords: Biped robot, Zero Moment Point (ZMP), Dynamic stability regulation, Cubic spline modeling, Compound path locomotion, Upper-body compensation.

1. INTRODUCTION

Bipedal robots, inspired by human locomotion, require advanced dynamic modeling and control strategies to maintain balance in the presence of instability and a high number of degrees of freedom [1]. Bipedal locomotion remains one of the most challenging problems in robotics, primarily because humanoid systems are underactuated, highly nonlinear, and sensitive to disturbances, while real-world terrains further increase the complexity of motion planning and stabilization [2]. Biped robots have numerous applications in fields such as medicine [3], agriculture [4], and industry [5]. Reference [6] addresses the limited attention given to energy consumption in legged robot design and proposes a novel energy-efficient four-bar linkage mechanism with passive joints and integrated energy storage. In [7], a parallel kinematic foot/ankle mechanism for humanoid robots is introduced, offering three rotational degrees of freedom and integrated force sensing to improve balance control and overall stability in biped systems. The Zero Moment Point (ZMP) method is widely used in biped robot control to ensure dynamic stability during standing and walking. By keeping the ZMP within the support polygon, the robot can avoid tipping and achieve stable locomotion [8]. A key advantage of this approach is its clear stability criterion and computational efficiency, which make it suitable for real-time gait generation and balance control [9]. In [10], the Linear Inverted Pendulum Model (LIPM) is used to derive the dynamic relationships among the Center of Mass (CoM), ZMP, and Capture Point for stable trajectory planning of a biped robot, while a disturbance-rejection feedback control strategy is employed to preserve stability during walking and phase transitions. In [11], a ZMP-based full-body control approach grounded in centroidal dynamics and accounting for manipulator dynamics is proposed to achieve stable transition from quadruped gait to biped locomotion in a quadruped manipulator robot. In [12], a hybrid ZMP–MPC control strategy based on the Linear Inverted Pendulum Model is proposed to achieve stable gait planning and improved dynamic balance in biped robots, demonstrating enhanced ZMP tracking performance in simulation. In [13], a Flexible Model Predictive

Control (FMPC) framework based on an enhanced flexible cart–table model that incorporates joint dynamics is introduced to generate bounded and stable gaits for humanoid robots. By using ZMP velocity as the control input and formulating linear CoM/ZMP constraints within a quadratic programming framework, the method ensures bounded trajectory generation and demonstrates robust performance in both simulation and real-robot experiments.

A biped robot can be naturally modeled as a hybrid switching system, in which the reference motion is generated through discrete transitions between locomotion phases such as single-support and double-support, thereby capturing the inherently discontinuous nature of walking dynamics [14]. In [15,16], an observer-based switching state-feedback control strategy is proposed for impulsive switched systems with uncertain inputs, providing reliable switching detection, accurate state estimation, and stability guarantees through Lyapunov- and LMI-based analysis. Despite these advances, a key gap remains in the literature: most existing biped control strategies are developed for fixed or idealized walking conditions and do not explicitly address locomotion over compound terrains, where flat, inclined, and stair-like surfaces require simultaneous handling of continuous trajectory evolution and discrete contact transitions. Moreover, the role of upper-body dynamics as an active stabilizing mechanism has not been fully integrated into phase-dependent ZMP regulation for such environments.

The main novelty of this paper lies in the development of a hybrid switching stability framework for a planar biped robot, where the admissible ZMP region is adaptively updated according to transitions between single-support and double-support phases. In addition, the upper-body dynamics are explicitly incorporated into the ZMP formulation as a compensatory mechanism, enabling corrective moments to be generated during phase switching. By combining switching control, cubic spline-based trajectory generation, and adaptive ZMP regulation, the proposed method provides a unified framework for improving trajectory tracking, disturbance rejection, and dynamic stability over compound walking surfaces.

The structure of this paper is organized as follows: Section 2 presents the dynamic modeling of the biped robot within a hybrid switching framework; Section 3 develops the upper-body-assisted ZMP-based

stability control method; Section 4 describes the proposed phase-dependent switching control strategy; and Section 5 presents simulation results to validate the effectiveness of the proposed approach.

2.Dynamic Modeling of the Biped Robot within a Hybrid Switching Framework

In this section, the biped robot is modeled within a hybrid switching framework to capture the coexistence of continuous body dynamics and discrete gait-phase transitions. The proposed formulation describes the robot motion during single-support and double-support phases, where the kinematic relations are used to generate feasible joint trajectories and the dynamic characteristics are preserved through phase-dependent switching. This modeling framework provides the basis for subsequent stability analysis and control design, enabling the robot to maintain coordinated motion over compound terrains while accounting for the abrupt changes in contact conditions that occur during walking.

2.1. Kinematic Modeling and Gait Parameter Definition

The kinematic analysis of the biped robot aims to determine joint configurations based on the prescribed horizontal and vertical trajectories of key points, namely the hip and ankle. To ensure smooth and dynamically feasible motion throughout a walking cycle, cubic spline interpolation is employed to generate continuous and twice-differentiable trajectories. This guarantees smooth variations in position, velocity, and acceleration profiles, which are essential for stable locomotion. After defining the time-dependent hip (x_h, z_h) and ankle (x_a, z_a) positions, the foot orientation relative to the ground is computed to accurately model foot–ground interaction during heel-strike and toe-off phases. With the hip position, ankle position, and foot angle specified, the inverse kinematics problem is solved using a simplified two-link leg model consisting of the thigh and shank segments. Based on known link lengths and geometric constraints between the hip, knee, and ankle joints, the corresponding joint angles are analytically derived. These joint trajectories are subsequently used as reference inputs for the control system to generate realistic walking motion while preserving dynamic balance.

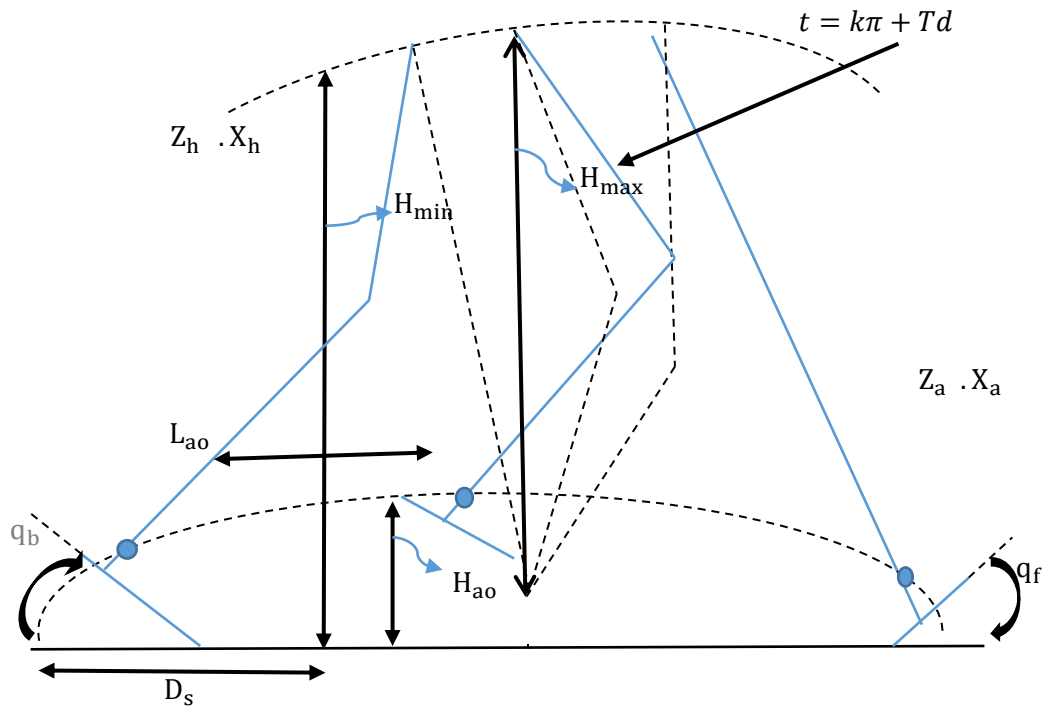


Figure 1. Kinematic model and gait parameters of the planar biped robot.

To accurately characterize the gait behavior of the biped robot, the essential kinematic parameters are defined as follows,

The hip position is expressed in a fixed coordinate frame attached to the stance foot and represented by (x_h, z_h). During the double-support phase, the horizontal hip displacement is bounded by two critical points, x_{Sd}, corresponding to the onset of double support, and x_{ed}, marking its termination. These parameters describe the forward progression of the robot's center of mass throughout the transition phase.

The swing ankle trajectory is defined by its horizontal and vertical coordinates (x_a, z_a) , governing foot clearance and step advancement. Temporal characteristics include the total gait cycle time Tc, the double-support duration T_d, and the time instant Tm at which the ankle reaches its peak height. Spatial descriptors such as the maximum ankle elevation H_{ao}, the horizontal travel to peak height L_{ao}, and the step length D_s determine the geometric structure of the step. Additionally, foot orientation and terrain interaction are

captured by the lift-off angle q_b, touch-down angle q_f, initial and final ground slopes (q_{gs}, q_{gf}), the overall terrain inclination k, and the stair riser height h_{st}.

Collectively, these parameters provide a comprehensive representation of the spatial, temporal, and terrain-dependent features of the gait, forming the foundation for trajectory planning and dynamic stability control.

As illustrated in Figure 2, the ankle angle on an inclined surface is defined by the following equation,

$$\theta_a(t) = \begin{cases} \lambda - q_{gs} & t = kT_c \\ \lambda - q_b & t = kT_c + T_a \\ \lambda + q_f & t = (k + 1/2)T_c \\ \lambda + q_{gf} & t = (k+1)T_c + T_a \end{cases} \quad (1)$$

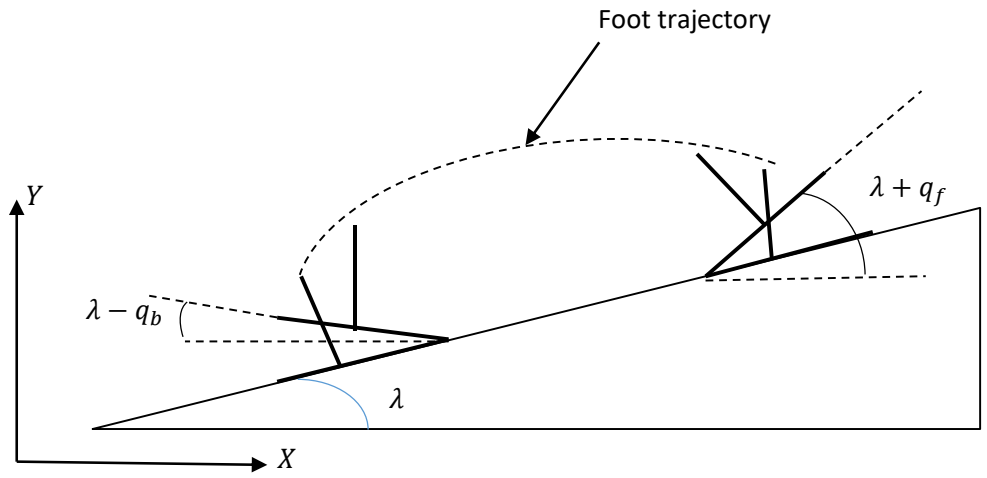


Figure 2. Foot angle formulation and trajectory on an inclined surface

The expressions for the foot angle on a flat surface and on a stair can be directly derived by setting $\lambda = 0$ n the corresponding inclined-surface relations. To ensure smooth rotational motion, boundary conditions are imposed such that the angular velocity is zero at both the beginning and the end of the swing phase,

$$\dot{\theta}(t_0) = 0, \quad \dot{\theta}(t_f) = 0 \quad (2)$$

The horizontal displacement of the ankle during the swing phase is modeled using a cubic polynomial to guarantee continuity in position and velocity,

$$x_{ahor}(t) = \begin{cases} kD_s & t = kT_c \\ kD_s + l_{an} \sin q_b + l_{af}(1 - \cos q_b) & t = kT_c + T_a \\ kD_s + L_m & t = kT_c + T_m \\ (k+1)D_s - l_{an} \sin q_f - l_{ab}(1 - \cos q_f) & t = (k+1)T_c \\ (k+1)D_s & t = (k+1)T_c + T_a \end{cases} \quad (3)$$

The polynomial coefficients are determined by applying the following boundary conditions,

$$\dot{x}_a(t_0) = 0, \quad \dot{x}_a(t_f) = 0 \quad (4)$$

For locomotion on an inclined plane, the effective forward displacement of the ankle is adjusted according to the terrain slope parameter. Accordingly, the horizontal progression is modified as follows,

$$x_{adec}(t) = \begin{cases} kD_s \cos\lambda - (l_{an} \sin\lambda) & t = kT_c \\ ((kD_s + l_{af}) \cos\lambda) - (l_{af} \cos(q_b - \lambda)) + (l_{an} \sin(q_b - \lambda)) & t = kT_c + T_a \\ (kD_s + L_{ao}) \cos\lambda & t = kT_c + T_m \\ ((k+1)D_s - l_{ab}) \cos\lambda + l_{ab} \cos(q_f + \lambda) - l_{an} \sin(q_f + \lambda) & t = (k+1)T_c \\ ((k+1)D_s \cos\lambda) - (l_{an} \sin\lambda) & t = (k+1)T_c + T_a \end{cases} \quad (5)$$

This formulation ensures geometric consistency between the swing trajectory and the inclined ground surface.

During stair traversal, the horizontal step length is maintained constant to preserve regular gait progression, while the vertical displacement accounts for the stair height. The corresponding relation is expressed as,

$$X_{ahor}(t) = \begin{cases} h_{gs} + l_{an} & t = kT_c \\ h_{gs} + l_{af} \sin q_b + l_{an} \cos q_b & t = kT_c + T_a \\ H_{st} & t = kT_c + T_m \\ h_{gs} + l_{ab} \sin q_f + l_{an} \cos q_f & t = (k+1)T_c \\ h_{gs} + l_{an} & t = (k+1)T_c + T_a \end{cases} \quad (6)$$

This approach guarantees smooth and stable foot placement during step climbing.

To ensure adequate ground clearance during the swing phase, the vertical trajectory of the ankle is defined using a smooth polynomial profile, expressed as:

$$Z_{adec}(t)$$

$$= \begin{cases} kD_s \sin\lambda - (l_{an}\cos\lambda) & t = kT_c \\ ((kD_s + l_{af})\sin\lambda) + (l_{af}\sin(q_b - \lambda)) + (l_{an}\cos(q_b - \lambda)) & t = kT_c + T_a \\ (kD_s + L_{ao})\sin\left(\frac{\pi}{2}\right) + H_{ao}\cos\lambda & t = kT_c + T_m \\ ((k+1)D_s - l_{ab})\sin\lambda + l_{ab}\cos\left(\frac{\pi}{2} - (q_f + \lambda)\right) + l_{an}\sin(q_f + \lambda) & t = (k+1)T_c \\ ((k+1)D_s\sin\lambda) + (l_{an}\cos\lambda) & t = (k+1)T_c + T_a \end{cases} \quad (7)$$

This formulation guarantees sufficient foot elevation while maintaining continuity in velocity and acceleration. For stair-climbing motion, the vertical ankle trajectory is modified to account for the step elevation, and is given by,

$$z_{stair}(t) = \begin{cases} (k-1)h_{st} + l_{an} & t = kT_c, \\ (k-1)h_{st} + l_{an} & t = kT_c + T_a, \\ l_{an}\cos q_b + l_{ab}\sin q_b + \cdots & t = kT_c + T_a, \\ kh_{st} + H_{st} & t = kT_c + T_m, \\ (k+1)h_{st} + l_{ab}\sin q_f + \cdots & t = (k+1)T_c, \\ l_{an}\cos q_f & t = (k+1)T_c + T_a, \end{cases} \quad (8)$$

where h_{st} denotes the stair height. This modification enables safe and stable foot placement during stair traversal.

The hip trajectory governs the global motion of the robot's center of mass (CoM) and plays a crucial role in maintaining dynamic stability throughout the gait cycle. The vertical motion of the hip is defined using a three-point spline interpolation constructed from the mid-stance height, the maximum height at the swing mid-point, and the terminal stance height. This formulation ensures smooth vertical CoM evolution during walking,

$$Z_{h,Hor} = \begin{cases} H_{hmin} & t = kT_c \\ H_{hmax} & t = kT_c + 0\cdot 5(T_c - T_a) \\ H_{hmin} & t = (k+)T_c\{ \end{cases} \quad (9)$$

For inclined surfaces, the hip height is further adjusted according to the terrain inclination angle to preserve geometric consistency and balance,

$$z_{hdec} = \begin{cases} (\boldsymbol{kD_s + x_{sd}})\,\boldsymbol{sin\,\lambda} + (\boldsymbol{H\,cos\,\lambda_{hmin}} & \boldsymbol{t = kT_c} \\ (\boldsymbol{kD_s + x_{sd}})\,\boldsymbol{sin\,\lambda} + (\boldsymbol{H\,cos\,\lambda_{hmax}} & \boldsymbol{t = kT_c +\cdot (T_c - T_a)} \\ ((\boldsymbol{k+1})\boldsymbol{D_s + x_{sd}})\,\boldsymbol{sin\,\lambda} + (\boldsymbol{H\,cos\,\lambda_{hmin}} & \boldsymbol{t = (k+1)T_c\{} \end{cases} \quad (10)$$

In stair-climbing scenarios, the vertical hip trajectory is modified to account for the step elevation,

$$z_{stair} = \begin{cases} (k-1)h_s + H_{min} & t = kT_c, \\ kh_s + H_{max} & t = kT_c + 5(T_c - T_d), \\ kh_s + H_{min} & t = (k+1)T_c, \end{cases} \quad (11)$$

The horizontal progression of the hip corresponds to one step length S per gait cycle and is initially defined as,

$$x_{hor}(t) = \begin{cases} kD_s + x_{ed} & t = kT_c \\ ((k+1)D_s - x_{sd} & t = kT_c + T_a \\ ((k+1)D_s + x_{ed} & t = (k+1)T_c \end{cases} \quad (12)$$

To guarantee smooth motion and avoid abrupt transitions, this trajectory is subsequently refined using spline interpolation.

2.2. Lower-Limb Inverse Kinematic Formulation

Figure 3, illustrates the planar configuration of the biped robot during a walking phase, showing the relative positioning of the hip and both legs in the sagittal plane. The geometric relationships between the links form the basis for deriving the analytical inverse kinematics used in joint angle computation.

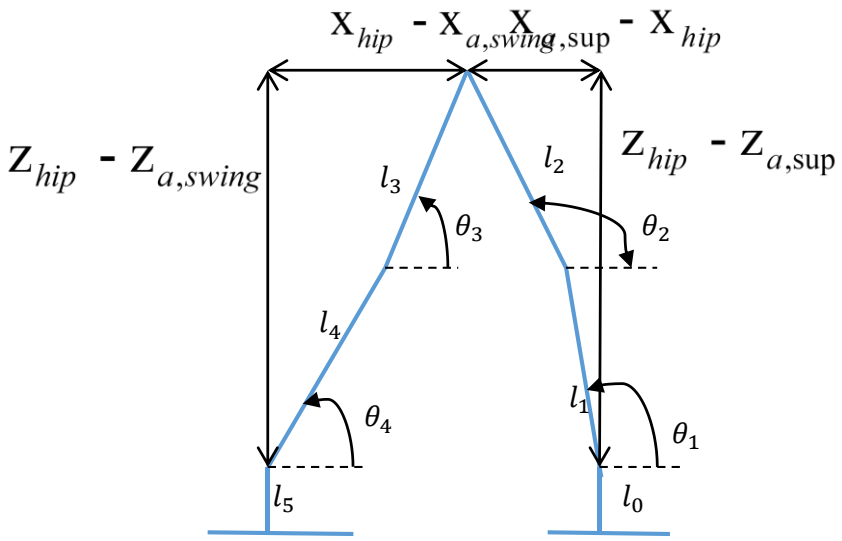


Figure 3. Geometric configuration of the planar biped robot in the sagittal plane.

The inverse kinematics of each leg is derived analytically by modeling the thigh and shank as a planar two-link mechanism operating in the sagittal plane. Let (x_h, z_h) denote the hip coordinates and (x_a, z_a) represent the ankle position for both stance and swing legs. The relative hip–ankle vectors are defined as,

$$
\begin{aligned}
x_1 &= \mathrm{x}\text{-}\,\mathrm{x}_{hip_{a,sup}} \\
z_1 &= \mathrm{z}_{hip} - \mathrm{z}_{a,sup} \\
x_2 &= \mathrm{x}_{hip} - \mathrm{x}_{a,swing} \\
z_2 &= \mathrm{z}_{hip} - \mathrm{z}_{a,swing}
\end{aligned}
\tag{13}
$$

Applying the geometric law of cosines, the auxiliary variables,

$$
\begin{aligned}
c_1 &= (X_1^2 + Z_1^2 - l_2^2 - l_3^2)/(2l_2l_3) \\
c_2 &= (X_2^2 + Z_2^2 - l_5^2 - l_6^2)/(2l_5l_6)
\end{aligned}
\tag{14}
$$

are introduced to compute the knee configuration. To enhance numerical robustness and prevent infeasible solutions due to modeling or measurement uncertainties, these terms are saturated within the interval $[-1,1]$. The remaining joint angles are then obtained through standard geometric decomposition,

$$\theta_1 = \pi/2 - (atan2(Z_1, X_1) - atan2(l_3 * sqrt(1 - c_1^2), l_2 + l_3 * c_1))$$
$$\theta_2 = \theta_1 - atan2(sqrt(1 - c_1^2), c_1) \quad (15)$$

for the swing leg,

$$\theta_4 = \pi/2 - (atan2(Z_2, X_2) - atan2(l_4 * sqrt(1 - c_2^2), l_3 + l_4 * c_2))$$
$$\theta_3 = \theta_4 - atan2(sqrt(1 - c_2^2), c_2) \quad (16)$$

for the stance leg. The robot is modeled as a seven-link planar mechanism with revolute hip, knee, and ankle joints. Link dimensions are selected according to anthropometric proportions to ensure realistic motion characteristic.

3. ZMP-Based Control Using the Upper Body

In this section, a ZMP-based dynamic stability control strategy incorporating upper-body compensation is developed for the biped robot traversing a composite walking path consisting of flat terrain, inclined planes, and stair steps. For each contact phase, the admissible ZMP stability region is first determined according to the corresponding support polygon. When the computed ZMP approaches or tends to leave this stable region, the torso is actively utilized as a compensatory mass by adjusting its angular posture, thereby generating corrective moments that relocate the ZMP within the allowable bounds.

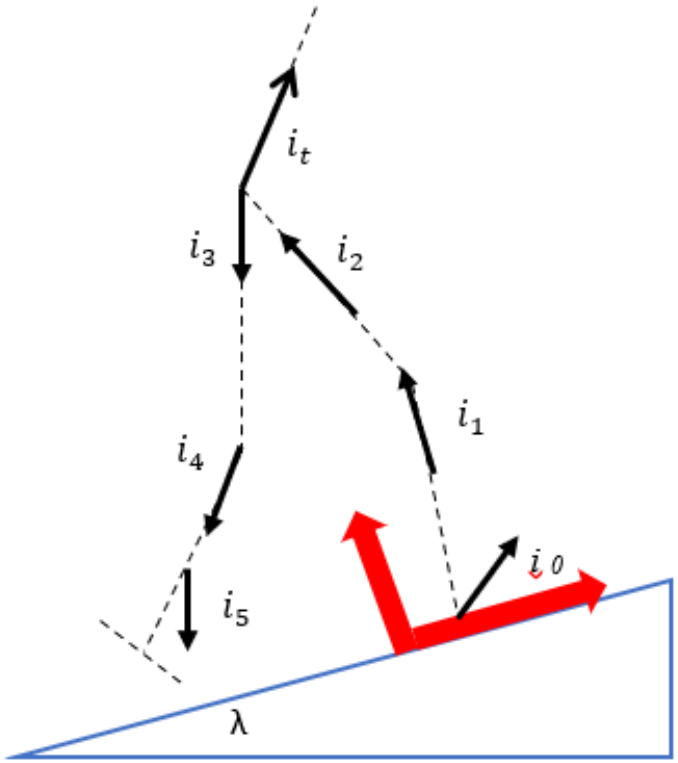


Figure 4. illustrates the assumed unit vectors employed for defining the position vectors required in the dynamic formulation.

Figure 4, illustrates the geometric configuration considered in the ZMP formulation on an inclined surface. The robot is represented in the sagittal plane, and the ground-fixed coordinate frame aligned with the slope is shown to highlight the effect of terrain inclination on the dynamic equilibrium. The orientation of the body links relative to the inclined ground is depicted to emphasize how gravitational and inertial effects are projected onto the slope, which directly influences the ZMP location. This representation provides the basis for analyzing stability over inclined terrain within the proposed control framework.

Consistent with human locomotion principles, the Zero Moment Point (ZMP) constitutes one of the most fundamental stability criteria for biped robots. The ZMP is defined as the point on the ground where the resultant moment of all inertial and gravitational forces becomes zero, ensuring dynamic balance during motion.

$$x_{\mathrm{ZMP}} = \frac{\sum_{i=1}^{n} m_i \,(g\cos\lambda + \ddot{z}_i)x_i - \sum_{i=1}^{n} m_i \,(g\sin\lambda + \ddot{x}_i)z_i - \sum_{i=1}^{n} I_i\,\ddot{\theta}_i}{\sum_{i=1}^{n} m_i \,(g\cos\lambda + \ddot{z}_i)} \tag{17}$$

where the horizontal and vertical accelerations correspond to the translational motion of each link's mass center in the global coordinate frame, and the angular acceleration is obtained from the interpolated joint trajectories. The surface inclination parameter is also incorporated to account for walking on sloped terrain. This formulation highlights that the ZMP is influenced by both translational and rotational dynamics of the robot, as well as by environmental geometry. In general, two ZMP formulations are considered depending on the walking condition: one corresponding to level or inclined surfaces, and another specifically adapted for stair-climbing scenarios. These formulations provide the foundation for the proposed upper-body-assisted stability regulation strategy developed in this section.

The admissible ZMP stability regions are derived from the geometric structure of the support polygon corresponding to each walking phase. Since the contact conditions vary between single-support and double-support intervals, the feasible ZMP domain must be defined in a phase-dependent manner. During the double-support phase, the stability region is determined by the convex hull formed by the contact areas of both feet, resulting in an enlarged admissible domain. In contrast, during the single-support phase, the feasible region reduces to the support area of the stance foot only, leading to a narrower stability margin. This phase-based characterization ensures an accurate representation of the robot–ground interaction throughout the gait cycle.

Figure 5, illustrates the temporal evolution of the feasible ZMP region over half of a walking cycle. The horizontal axis represents time, while the vertical axis indicates the admissible ZMP position range. The shaded areas correspond to the allowable stability intervals during the double-support and single-support phases. Points $A, B,$ and C denote representative boundary conditions of the ZMP trajectory at key transition instants. The figure highlights how the admissible region expands during double support and contracts during single support, emphasizing the importance of phase-aware stability monitoring.

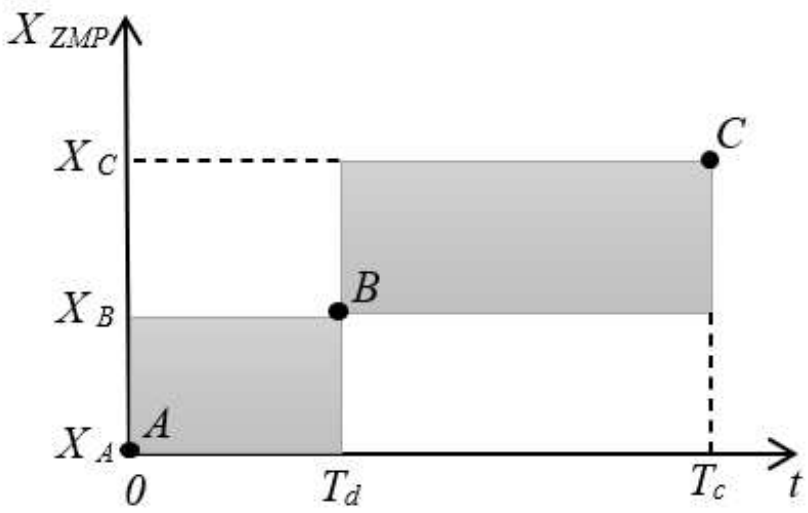


Figure 5. Temporal evolution of the admissible ZMP stability region over half of a gait cycle.

Figure 6 depicts the spatial configuration of the robot corresponding to these key instants. The positions labeled A, B, and C represent characteristic postures during different contact phases within the half-cycle. These configurations define the geometric limits of the support polygon and consequently determine the ZMP stability boundaries. The figure provides a physical interpretation of the temporal stability regions shown in Figure 5, linking the admissible ZMP domain to the robot's actual foot placement and body posture.

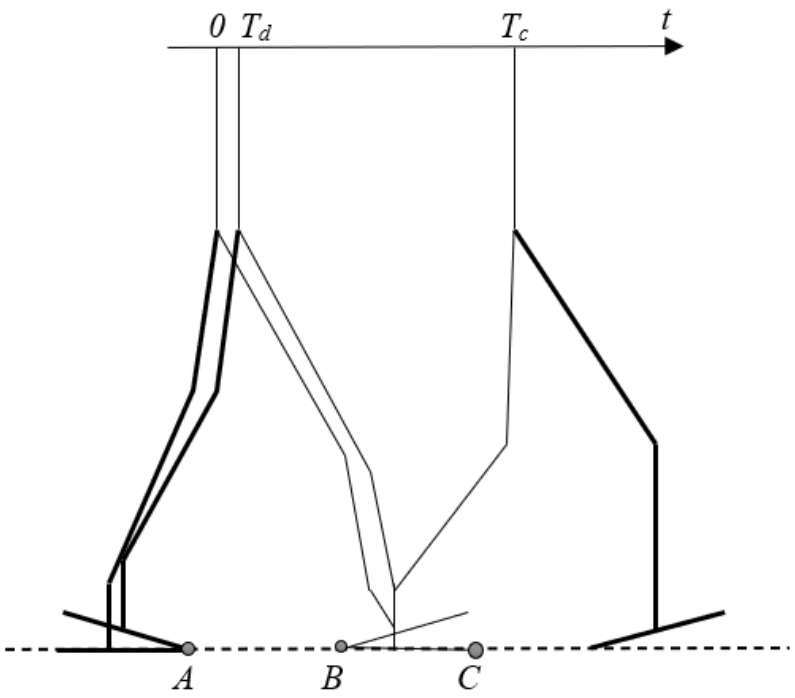


Figure 6. Spatial configurations defining the ZMP stability boundaries during gait phases.

To enhance robustness in practical implementation, a conservative safety margin is introduced within the nominal support polygon. This margin accounts for modeling uncertainties, sensor noise, and possible variations in foot–ground contact conditions, thereby improving reliability of the ZMP-based stability control during real locomotion.

4. Control Strategy

The proposed stability controller is formulated as a phase-dependent switching ZMP regulation framework with upper-body actuation. The main objective is to guarantee that the Zero Moment Point (ZMP) remains inside the admissible support region throughout the gait cycle while preserving nominal locomotion performance whenever possible. At each control instant, the computed ZMP position $x_{ZMP}(t)$ is compared with the phase-dependent admissible interval derived from the support polygon. The controller operates in two distinct modes:

A. Nominal Mode (ZMP Inside Stability Region)

When the ZMP satisfies,

$$\text{if} \quad x_{\text{ZMP, min}}(t) \leq x_{\text{ZMP}}(t) \leq x_{\text{ZMP, max}}(t) \tag{18}$$

the system is considered dynamically stable. In this case, no corrective action is required, and the torso follows its preplanned spline-based trajectory,

$$\ddot{\beta}^{\text{des}}(t) = \ddot{\beta}^{\text{nominal}}(t), \quad \beta(t) \leftarrow \text{spline-interpolated reference.} \tag{19}$$

This ensures smooth and energy-efficient locomotion without unnecessary upper-body actuation.

B. Corrective Mode (ZMP Outside Stability Region)

$$\text{if} \quad x_{\text{ZMP}}(t) < x_{\text{ZMP,min}}(t) \quad \text{or} \quad x_{\text{ZMP}}(t) > x_{\text{ZMP,max}}(t) \tag{20}$$

where $S(t)$ denotes the admissible ZMP region, the controller switches to a corrective compensation mode. The torso angular acceleration is adjusted to generate a stabilizing moment that shifts the ZMP toward a safe reference location within the support polygon. Based on moment equilibrium about the desired ZMP location.

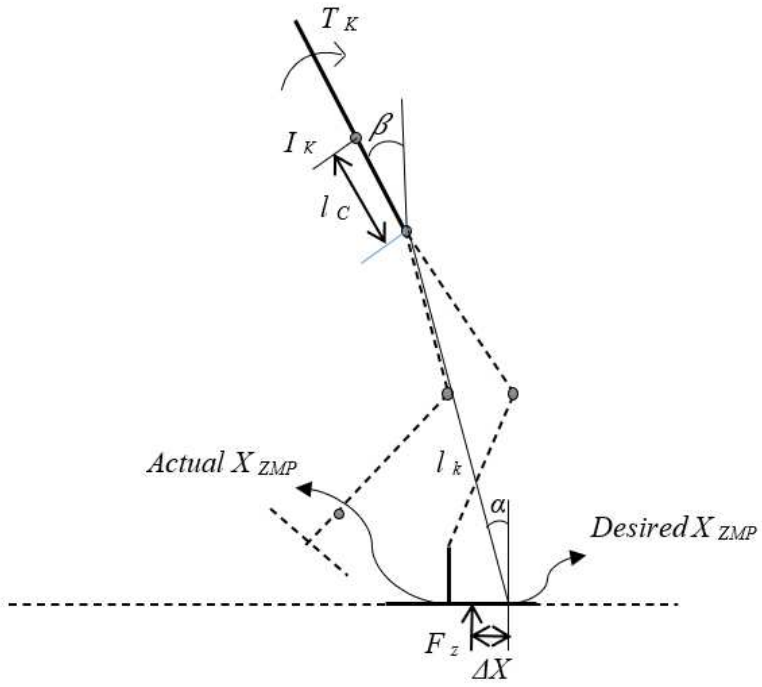


Figure 7. ZMP regulation via upper-body rotational compensation mechanism

Figure 7 illustrates the upper-body-based compensation mechanism employed for ZMP regulation. When a deviation occurs between the actual and desired ZMP positions, the torso is rotated to generate a corrective moment about the support foot. This rotational motion modifies the distribution of ground reaction forces, resulting in a controlled horizontal shift of the ZMP toward the admissible stability region.

The dynamic relation can be expressed as,

$$F\Delta x = I_k\ddot{\beta} + m_k l_k \cos(\beta - \alpha)\ddot{\beta} \tag{21}$$

Under typical walking conditions with moderate torso inclination $\Delta x = -e_{\text{ZMP}}, \quad F \approx mg$ he corrective acceleration becomes,

$$\ddot{\beta}^{\text{des}}(t) = \frac{mg \cdot e_{\text{ZMP}}(t)}{I_k + m_k l_k} \tag{22}$$

Where $e_{ZMP}(t)$ represents the ZMP tracking error relative to a safe internal reference. For computational efficiency, an equivalent torso inertia

$$I_{\text{torso}} = I_k + m_k l_k \tag{23}$$

is introduced, yielding the compact switching control law,

$$\ddot{\beta}^{\text{des}}(t) = \begin{cases} \ddot{\beta}^{\text{nominal}}(t), & \text{if } x_{\text{ZMP}} \in \mathcal{S}(t) \\ \dfrac{mg \cdot e_{\text{ZMP}}(t)}{I_{\text{torso}}}, & \text{otherwise} \end{cases} \tag{24}$$

To enhance robustness against modeling uncertainties and terrain disturbances, a proportional feedback gain $K_{ZMP}(t)$ is incorporated,

$$\ddot{\beta}^{\text{des}}(t) = K_{\text{ZMP}} \frac{mg \cdot e_{\text{ZMP}}(t)}{I_{\text{torso}} + m_k l_k \, cos(\beta - \alpha)}, \quad K_{\text{ZMP}} \in [0.2, 1.2] \tag{25}$$

The gain $K_{ZMP}(t)$ regulates the responsiveness of the corrective action and is tuned to balance rapid stabilization and oscillation suppression. Experimental tuning indicated that a moderate gain provides optimal ZMP convergence without inducing excessive torso motion.

5. Simulation Results

To assess the effectiveness of the proposed switching ZMP-based stability controller, comprehensive numerical simulations were conducted on a planar seven-link biped robot traversing a composite terrain composed of an inclined surface and a stair segment. The simulations were performed in MATLAB, where the complete kinematic and dynamic equations were implemented to compute joint trajectories, link velocities and accelerations, as well as the corresponding ZMP evolution over the gait cycle. Special emphasis was placed on the transitions between single-support and double-support phases to evaluate the responsiveness of the switching controller and its ability to preserve dynamic stability under varying terrain conditions.

Table I. Physical, Geometric, and Dynamic Parameters of the Biped Robot Model

$\mathbf{l_{sh}}$	$\mathbf{l_{Ti}}$	$\mathbf{l_{To}}$	$\mathbf{l_{an}}$	$\mathbf{l_{ab}}$	$\mathbf{l_{af}}$
45 cm	55 cm	65 cm	10 cm	10 cm	13 cm
$\mathbf{m_{Sh}}$	m_{Th}	m_{To}	m_{Fo}	D_s	T_c
5.7 kg	10 kg	40 kg	3.3 kg	50 cm	1 s
$\boldsymbol{T_d}$	T_m	H_{ao}	L_{ao}	x_{ed}	x_{sd}
0.2 s	0.5 s	28 cm	25 cm	23 cm	23 cm
$\boldsymbol{g_{gs}}$	g_{gf}	H_{min}	H_{max}	h_s	H_s
0	0	108 cm	110 cm	20 cm	20 cm
	$\mathbf{I_{shank}}$	$\boldsymbol{I_{tight}}$	$\boldsymbol{I_{torse}}$	$\boldsymbol{I_{foot}}$	
	0.1 kg m^2	0.8 kg m^2	1.4 kg m^2	0.1 kg m^2	

The physical, geometric, and inertial parameters of the robot used in the simulations are summarized in Table I. These parameters include link lengths, masses, inertias, gait timing variables, step length, swing-foot clearance, and terrain characteristics. The selected values ensure realistic anthropomorphic proportions and provide a dynamically consistent platform for validating the effectiveness of the proposed upper-body-assisted ZMP regulation strategy.

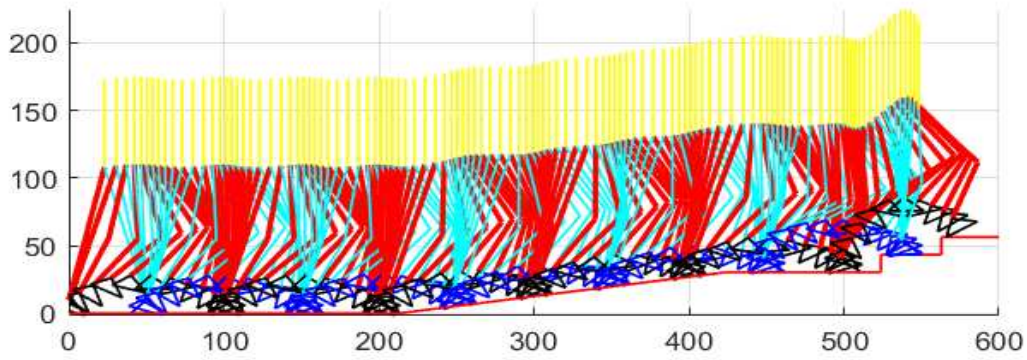


Figure 8. Time Evolution of Link Kinematics During Composite Terrain Locomotion

Figure 8 presents the kinematic response of the biped robot while traversing the composite terrain. The plotted curves represent the time evolution of link motions during successive gait cycles, including slope climbing and stair negotiation phases. The periodic patterns indicate consistent alternation between stance and swing phases, confirming proper synchronization of the lower limbs. The gradual increase in trajectory amplitude reflects the transition from flat terrain to inclined and stair segments. Despite terrain variations, the motion profiles remain continuous without abrupt discontinuities, demonstrating the effectiveness of the spline-based trajectory generation and the stability of the proposed switching control strategy. The absence of irregular spikes or oscillatory divergence confirms stable dynamic behavior throughout the simulation interval.

Figures 9(a–f) present the time evolution of the linear velocity components of the selected lower-limb links during the composite gait motion. The plotted curves correspond to representative segments of the biped robot, illustrating both horizontal and vertical velocity components throughout successive walking cycles. The velocity profiles exhibit clear periodic behavior associated with the alternating stance and swing phases. Peak values occur during the swing phase when forward propulsion and foot clearance are required, while reduced magnitudes are observed during stance intervals. The smooth and continuous nature of the velocity curves confirms the effectiveness of the spline-based trajectory generation in ensuring first-order continuity.

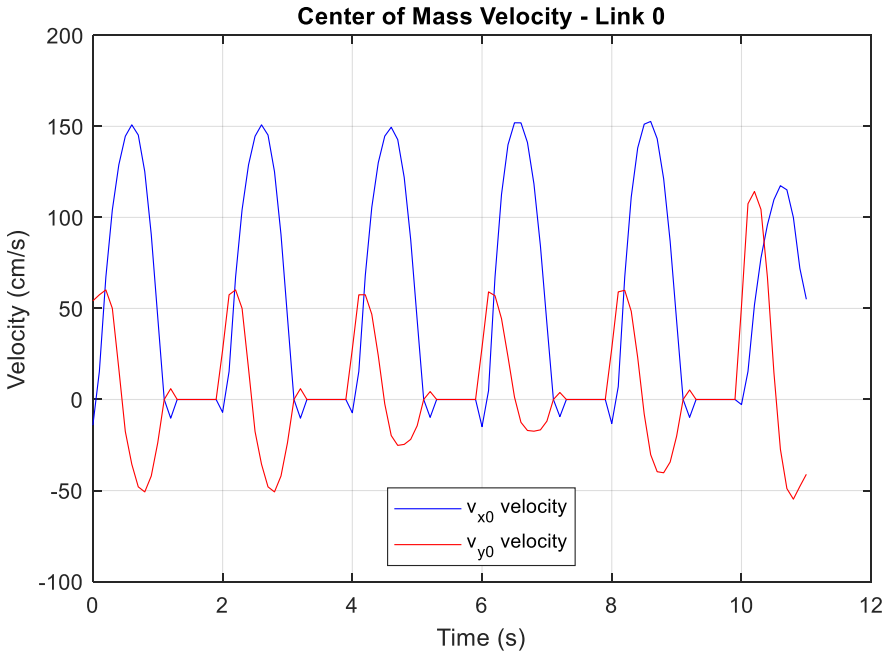


Figure 9(a). Velocity components of the right ankle (Link 0).

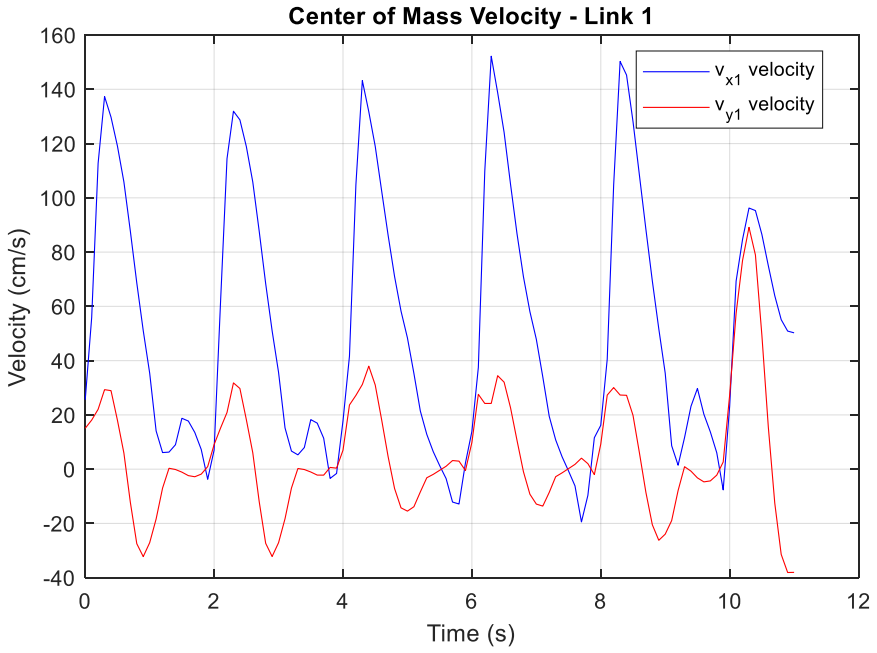


Figure 9(b). Velocity components of the right shank (Link 1).

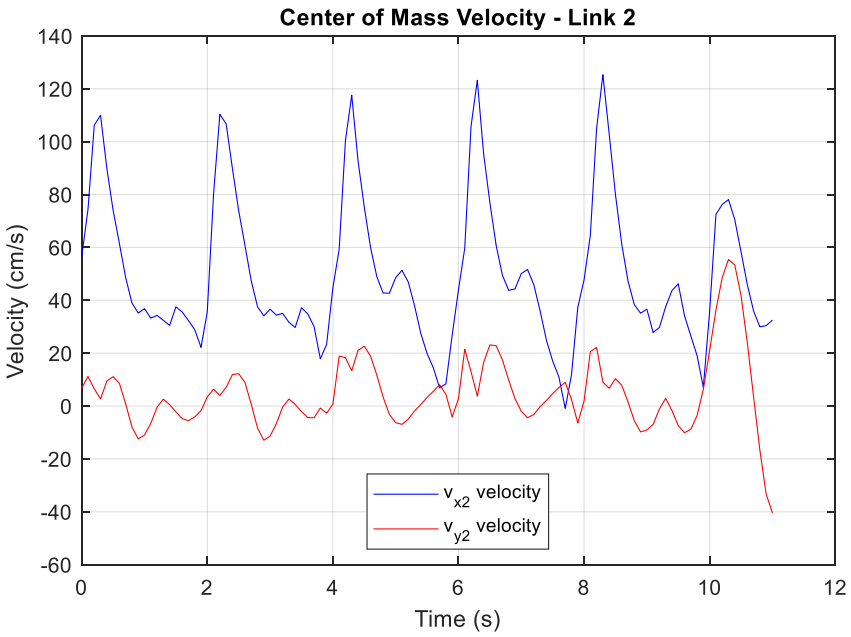


Figure 9(c). Velocity components of the right thigh (Link 2).

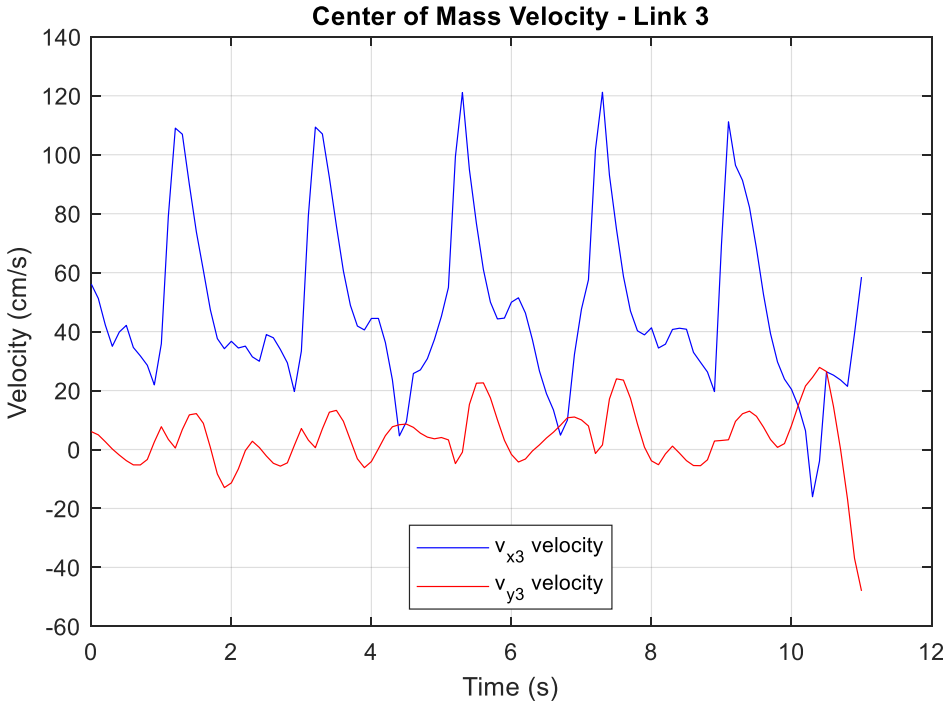


Figure 9(d). Velocity components of the left thigh (Link 3).

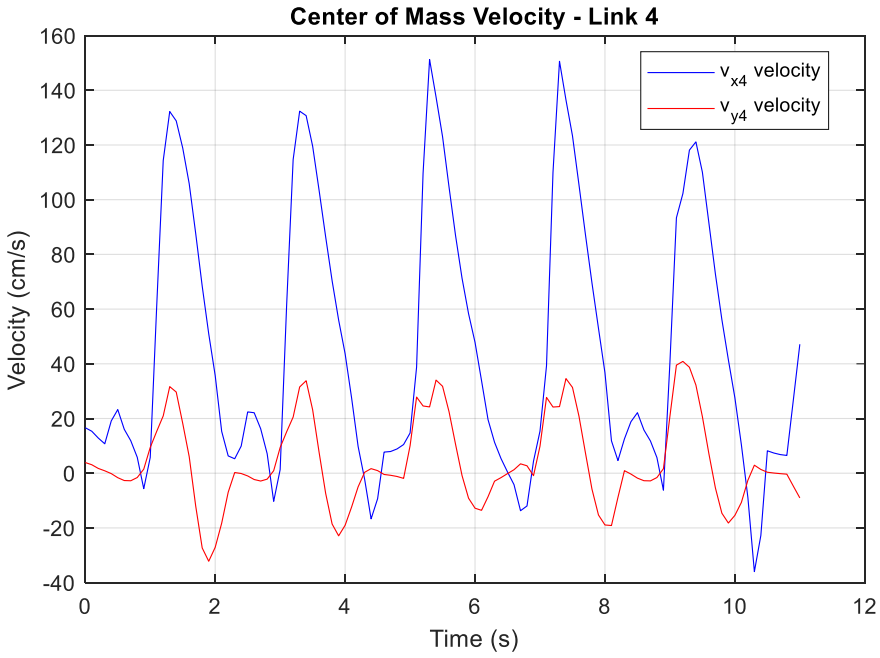


Figure 9(e). Velocity components of the left shank (Link 4).

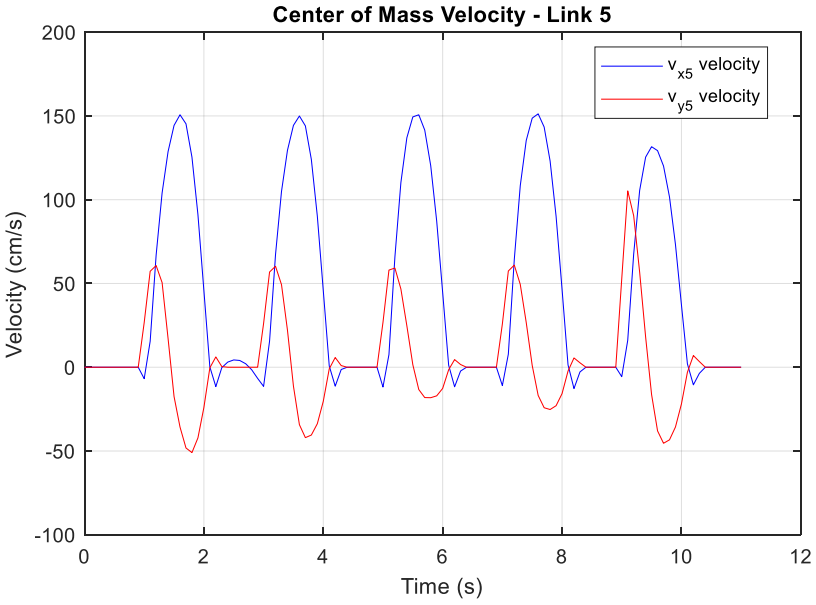


Figure 9(f). Velocity components of the left ankle (Link 5).

Figures 10(a–f) show the corresponding acceleration components of the same links. As expected, acceleration profiles exhibit higher dynamic variations compared to velocities, particularly during terrain transitions and foot-ground contact events. Nevertheless, the acceleration signals remain bounded and free

of impulsive discontinuities, indicating that the proposed switching ZMP control strategy does not introduce destabilizing dynamic shocks. The absence of irregular spikes confirms that the motion remains dynamically feasible and well-regulated throughout both single- and double-support phases.

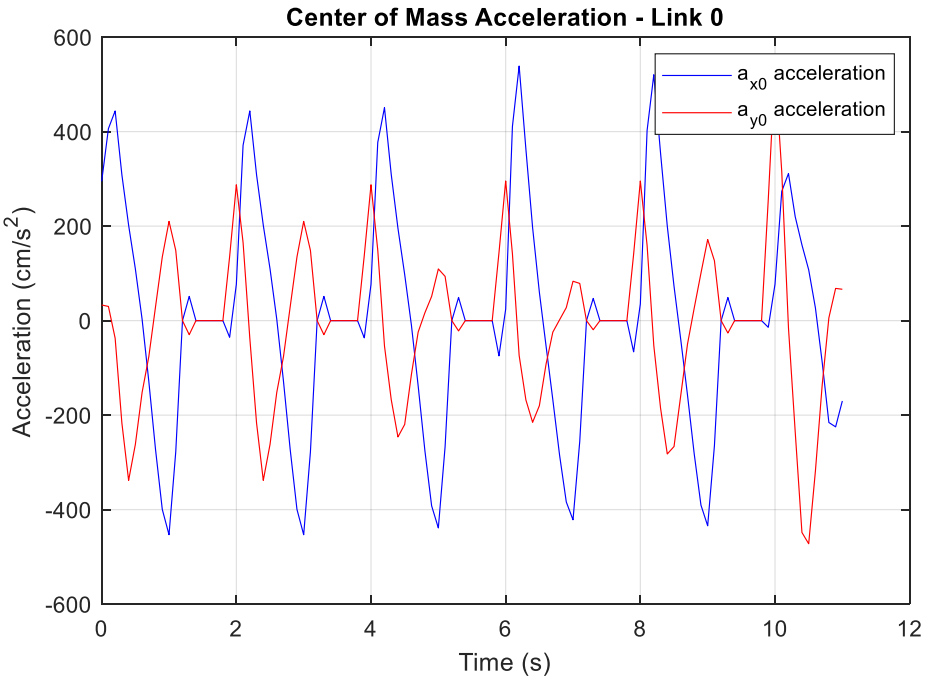


Figure 10(a). Acceleration components of the right ankle

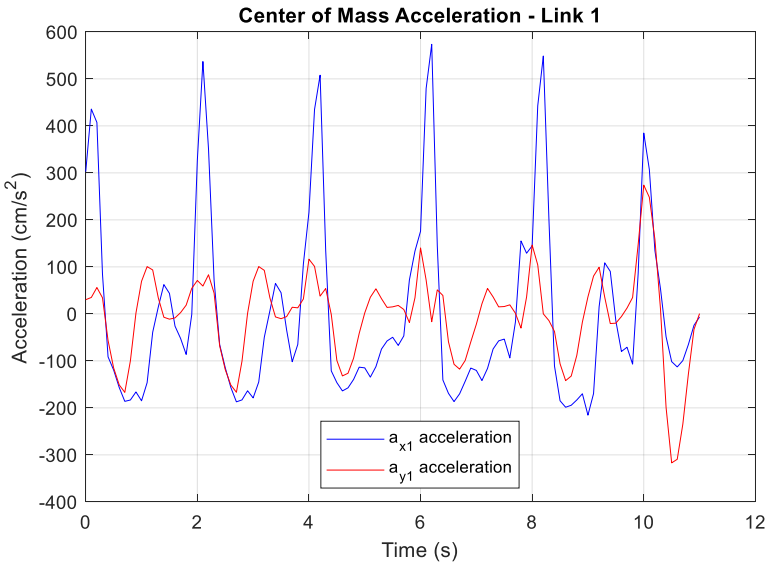


Figure 10(b). Acceleration components of the right shank

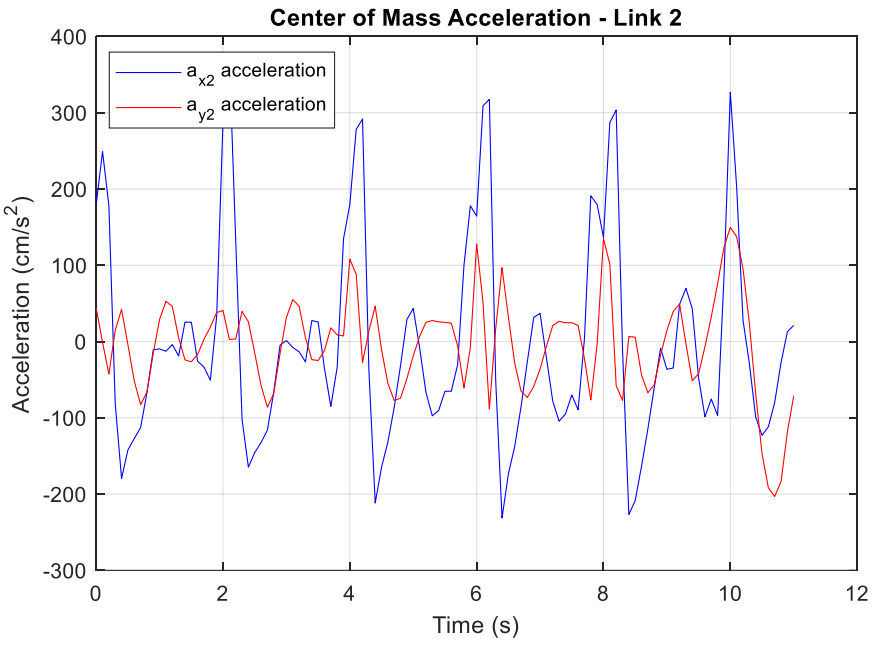


Figure 10(c). Acceleration components of the right thigh

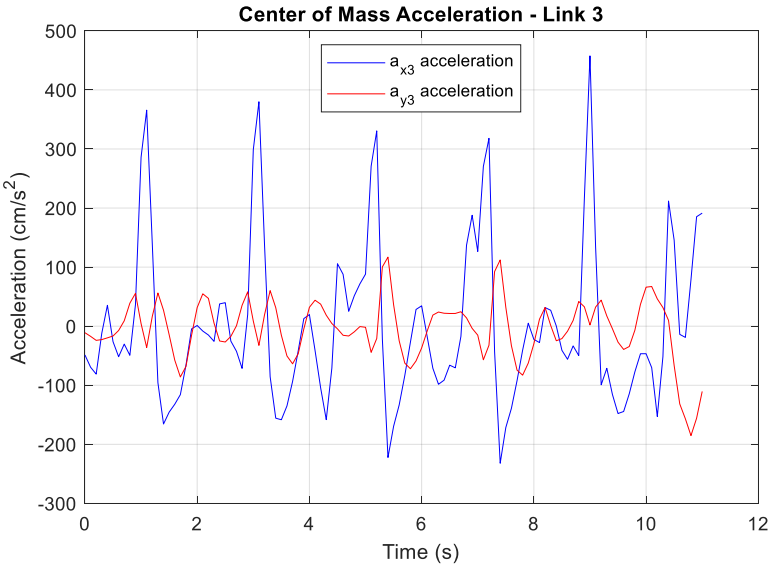


Figure 10(d). Acceleration components of the left thigh

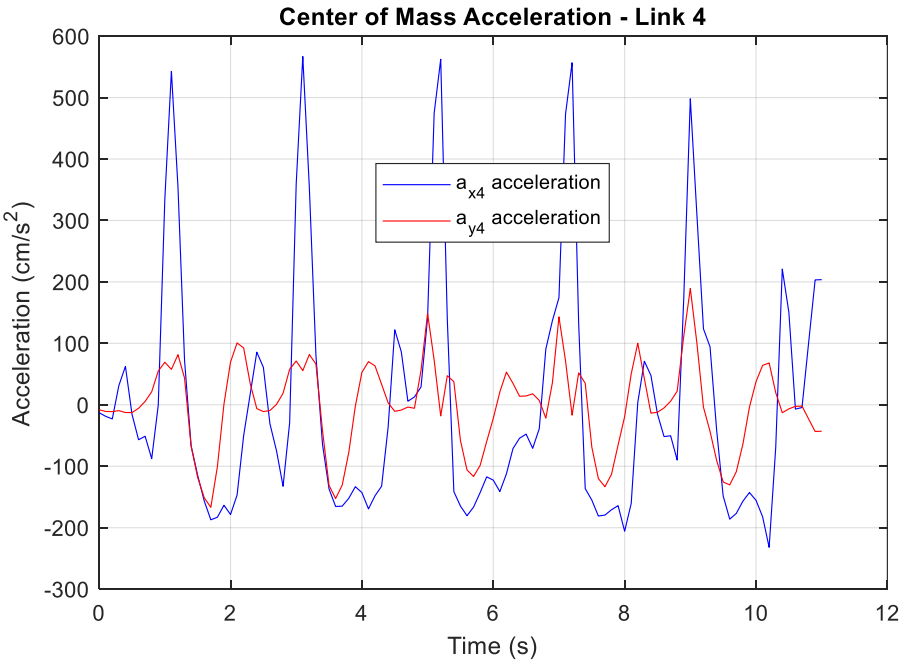


Figure 10(e). Acceleration components of the left shank

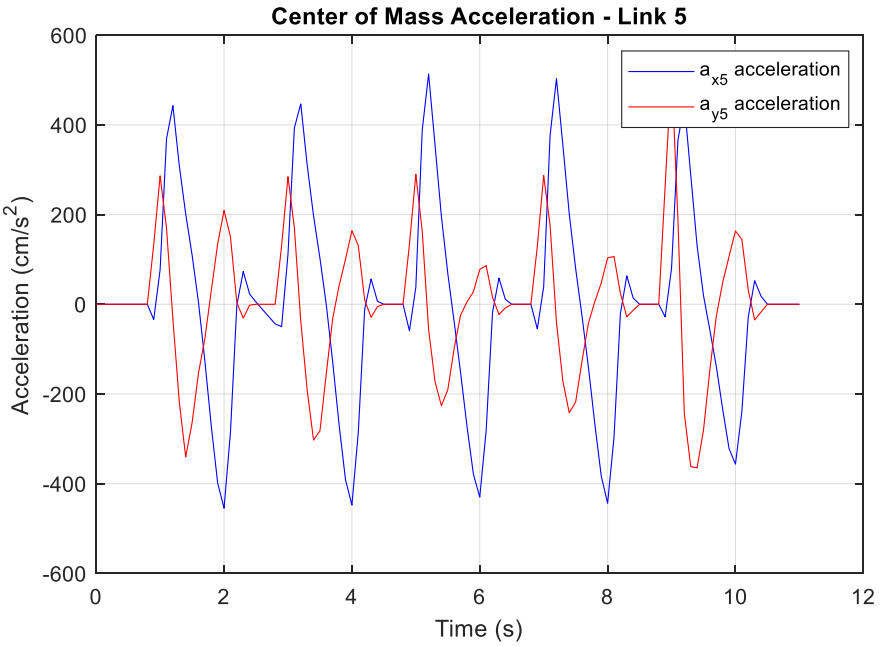


Figure 10(f). Acceleration components of the left ankle

As shown in Figure 11, the blue curve represents the Zero Moment Point (ZMP) trajectory of the biped robot during compound gait motion based on the method reported in [17]. The shaded regions denote the

admissible stability domains corresponding to the single- and double-support phases, illustrated in red and blue, respectively. It can be observed that the ZMP periodically approaches and, in certain intervals, slightly exceeds the stability boundaries, particularly during transitions between support phases. These deviations reflect reduced robustness and increased oscillatory behavior when the robot encounters terrain variations, highlighting the limitations of the baseline approach in maintaining strict dynamic stability.

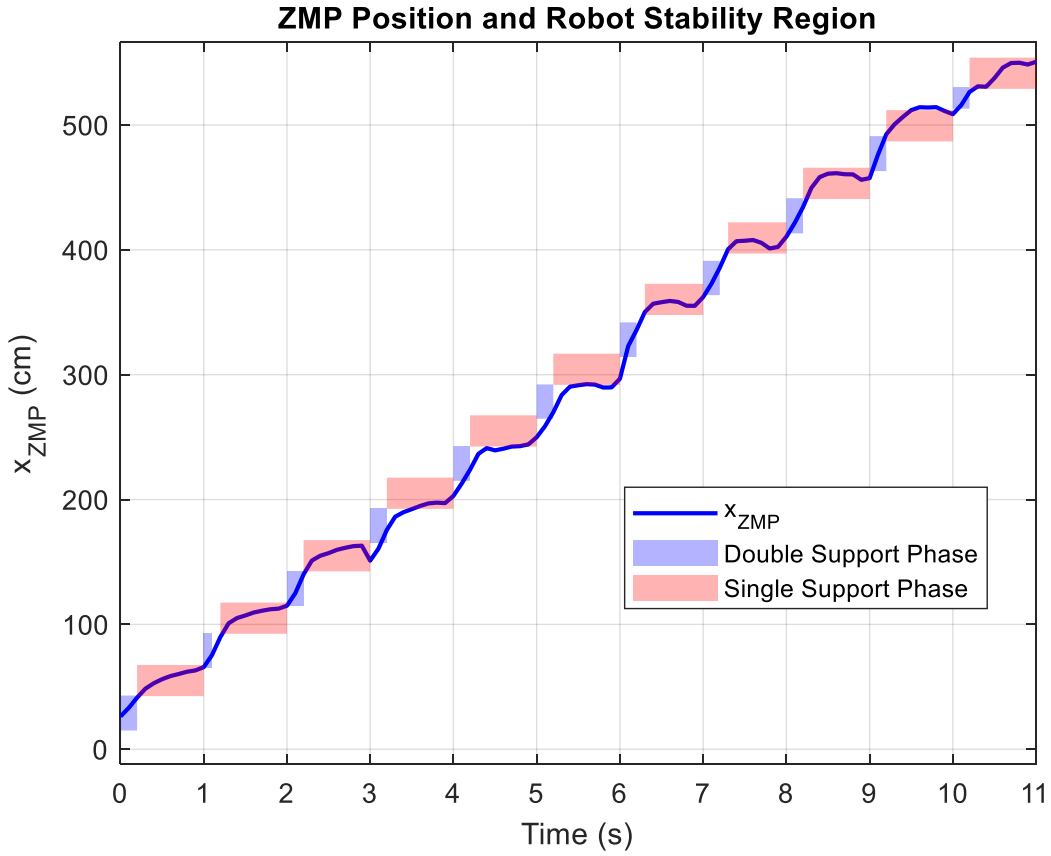


Figure 11. ZMP trajectory and stability region during compound gait motion using the baseline method of [17]

As illustrated in Figure 12, the proposed switching control strategy activates corrective action only when the ZMP deviation exceeds a predefined threshold of 3 cm from the stability boundary. This selective activation mechanism avoids unnecessary control effort, reduces excessive torso motion, and preserves nominal gait behavior during stable intervals. It can be clearly observed that, after applying the proposed controller, the ZMP trajectory remains strictly confined within or very close to the admissible stability

region throughout the entire walking cycle. Compared to the baseline method, the oscillation amplitude is noticeably attenuated, particularly during critical transitions between single- and double-support phases. This improvement demonstrates the effectiveness of the upper-body-based switching compensation in enhancing dynamic robustness and maintaining reliable balance over composite terrain conditions.

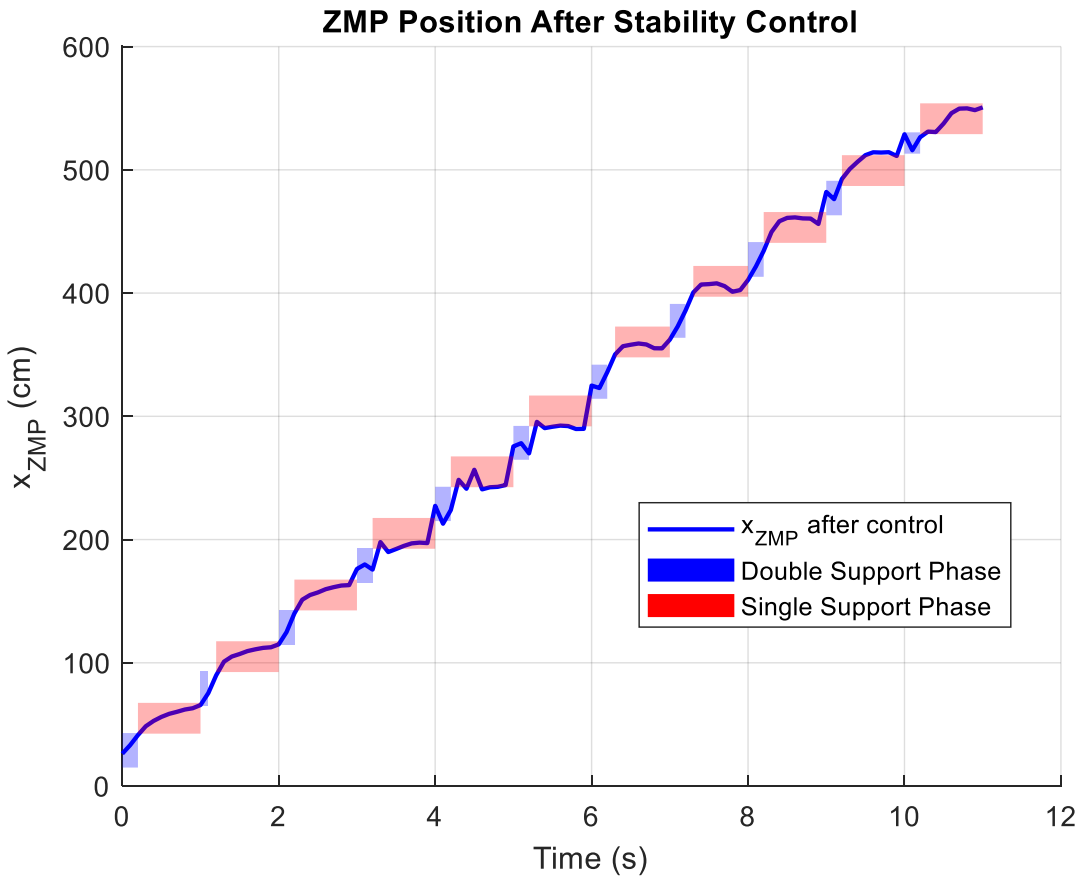


Figure 12. ZMP trajectory after applying the proposed switching upper-body compensation control strategy.

6. Conclusion

This paper presented a hybrid switching ZMP-based dynamic stability control framework for a planar biped robot traversing compound walking surfaces, including flat, inclined, and stair terrains. By explicitly modeling single- and double-support phase transitions and employing cubic spline interpolation for smooth joint trajectory generation, continuous and dynamically feasible locomotion was achieved. The incorporation of upper-body dynamics into the ZMP formulation, combined with selective switching

activation near stability boundaries, enabled effective compensatory torque generation and significant reduction of ZMP oscillations during terrain transitions. Simulation results confirmed that the proposed strategy enhances dynamic balance, maintains smooth and coordinated motion, and provides a robust and computationally efficient solution for stable biped locomotion over complex surfaces.

Acknowledgements

Arash Rahmani: Writing– review & editing, Supervision, Project administration. Soheil Sheikh Ahmadi: Writing review & editing, Supervision, Project administration, Formal analysis, Conceptualization. Mohammad Hatamnezhad: Writing– original draft, Validation, Methodology, Conceptualization

Funding

The authors did not receive support from any organization for the submitted work.

Ethics Approval and Consent to Participate

This study does not involve human participants or animals. Therefore, ethics approval and consent to participate are not applicable.

Competing Interests

The authors declare that they have no known financial or personal conflicts of interest that could have appeared to influence the work reported in this paper.

Consent for Publication

Not applicable.

Data Availability

The datasets generated during and/or analysed during the current study are available from the corresponding author on reasonable request.

Declaration of Generative AI and AI-assisted Technologies in the Writing Process

During the preparation of this manuscript, AI-assisted language tools were used solely for minor language refinement and readability improvement. All scientific content, analysis, and conclusions were developed by the authors. The authors have carefully reviewed and approved the final version of the manuscript and take full responsibility for its content.

REFERENCES

1. Al-Tameemi I, Amanuel O. Bipedal robots: A systematic review of dynamical models, balance control strategies, and locomotion methods. Journal of Robotics and Control (JRC). 2025 May 13;6(3):1240-54.

2. Ridwan W, Mysorewala MF. Survey of Bipedal Robot Control: A Functional Classification by Control Objectives. Journal of Robotics and Control (JRC). 2025 Nov 10;6(6):2676-96.

3. Niknezhad S., Moazemi Goudarzi A. Biomechanical Evaluation of Compliance Joint Knee Exoskeleton During Normal Gait. *IJE*, 2024; 37(10): 2099-2108. doi: 10.5829/ije.2024.37.10a.20.

4. Moshayedi A. J., Khan A. S., Geng K., Hu J., Kolahdooz A. Advancing Agricultural Practices: Analyzing the Role of Robotics in Corn Farming. IJE, 2025; 38(7): 1517-1532. doi: 10.5829/ije.2025.38.07a.07.

5. Srisuchinnawong A, Phongaksorn K, Ausrivong W, Manoonpong P. Adaptive bipedal robot walking on industrial pipes under neural multimodal locomotion control: Toward robotic out-pipe inspection. IEEE/ASME Transactions on Mechatronics. 2023 Jul 21;29(2):1205-16.

6. Mahmoodabadi M. J., Dresscher D., Stramigioli S. A New Mechanical Design for Legged Robots to Reduce Energy Consumption. IJE, 2020; 33(12): 2530-2537. doi: 10.5829/ije.2020.33.12c.14.

7. Liang Q., Wang Y. Flexible Foot/Ankle Based on PKM with Force/Torque Sensor for Humanoid Robot. IJE, 2011; 24(4): 377-386.

8. Khan MS, Mandava RK. A review on gait generation of the biped robot on various terrains. Robotica. 2023 Jun;41(6):1888-930.

9. Haldar AI, Pagar ND. Predictive control of zero moment point (ZMP) for terrain robot kinematics. Materials Today: Proceedings. 2023 Jan 1;80:122-7.

10. Gan C, Li Z, Ge Y, Lu M. COM trajectory planning and disturbance-resistant control of a bipedal robot based on CP-ZMP-COM dynamics. Journal of Zhejiang University-SCIENCE A. 2025 May;26(5):492-8.

11. Zhao C, Chen J, Ma T, Sun P, Luo X. A Quadruped Manipulator Robot that Achieves Bipedal Motion via ZMP Planning and Dynamic Control. InInternational Conference on Intelligent Robotics and Applications 2024 Jul 31 (pp. 171-182). Singapore: Springer Nature Singapore.

12. Wang P, Duan H, Yang L, Chen Y, Wang D, Liu S. Design of Bipedal Robot Motion Controller Based on ZMP Theory and MPC. InChina Intelligent Networked Things Conference 2025 Jun 10 (pp. 245-257). Singapore: Springer Nature Singapore.

13. Yang T, Tong Y, Zhang Z. Flexible model predictive control for bounded gait generation in humanoid robots. Biomimetics. 2025 Jan 6;10(1):30.

14. Li Y, Zhao Y. Improved impedance control technique for bipedal robot swing leg landing based on switching tree. Measurement and Control. 2025 Mar 29:00202940251324410.

15. Ahmadi SS, Hashemzadeh F, Badamchizadeh MA. Observer-based controller for impulsive switched systems with uncertain inputs. In2025 33rd International Conference on Electrical Engineering (ICEE) 2025 May 13 (pp. 1-5). IEEE.

16. Ahmadi SS, Hashemzadeh F, Badamchizadeh MA. Reduced order state estimation for a class of impulsive switched systems with unknown inputs. ISA transactions. 2024 Dec 1;155:171-83.

17. Mousavi PN, Nataraj C, Bagheri A, Entezari MA. Mathematical simulation of combined trajectory paths of a seven link biped robot. Applied Mathematical Modelling. 2008 Jul 1;32(7):1445-62.